16th European Signal Processing Conference (EUSIPCO 2008), Lausanne, Switzerland, August 25-29, 2008, copyright by EURASIP

VELOCITY ESTIMATION WITH 3D SPATIOTEMPORAL FILTERING OF SEQUENCES OF ULTRASOUND IMAGES: A FOURIER APPROACH

Adrien MARION and Didier VRAY

CREATIS-LRMN, CNRS, UMR5220, INSERM, U630
INSA-LYON, UCBL, F-69621 Villeurbanne, France
phone: + (33) 4 72 43 87 86, fax: + (33) 4 72 43 85 26
email: adrien.marion@creatis.insa-lyon.fr, didier.vray@creatis.insa-lyon.fr

ABSTRACT

Blood velocity estimation is required in many clinical applications. Ultrasonic imaging is often used to reach this goal. This article presents a velocity vector estimation method from ultrasonic imaging. It complements Doppler imaging, which has several limitations. Our method is based on spatiotemporal filtering to estimate the apparent velocity vector for each pixel of the sequence of B-mode imaging. Jacobson [1] then Porat [2] showed that the three-dimensional Fourier transform of a sequence in translation is zero except for a plane plane passing through the origin. The slope of this plane is proportional to the velocity components v_x and v_y. We suggest to design a bank of filters in order to estimate this slope then deduce the velocity vector. The method was applied to sequences of ultrasound images of calibrated flow in a vessel (mean velocity < 1 mm/s). The velocity estimates obtained are exhibited mean errors inferior to 9%. Results are presented as dynamic cartography and dense fields of velocity vectors. Associated velocity profiles show good agreement with the theoretical parabolic profile of laminar flow.

1. INTRODUCTION

A number of clinical applications require estimating blood velocity. Ultrasonic imaging is often used to reach this goal in real-time imaging. Ultrasonic images make up a specific pattern, called speckle, due to the image formation process. Indeed, an image results from the backscattering of ultrasonic waves by a set of scatterers randomly distributed in biological tissues or in the blood. However, the impulse response (Point Spread Function) of the imaging system is known and therefore image processing methods can be adapted.

Widespread Doppler techniques are a reference to estimate blood velocities. Kasai [3] has notably developed a real-time autocorrelation estimator that evaluates the average phase shift related to the axial velocity. However, Doppler suffers from a number of limitations:

- poor estimation of low velocities
- the spatial resolution is limited
- the flow orientation must be known to estimate velocity

Jensen and Munk [4] explored the use of lateral oscillations (transverse spatial modulation) to study and quantify the influence of transverse motion on the received signals. Block matching techniques, called speckle tracking in ultrasonic imaging, have been widely studied [5]. The principle is based on the maximization of a similarity measure between two blocks from two successive images. To avoid decorrelation during motion, a deformation model has also been proposed [6]. Other methods that exploit the statistics of the ultrasonic image recently appeared. They associate velocity and decorrelation [7, 8].

The spatiotemporal-frequency (STF) approach is well known to estimate motion in image sequences [9]. Jacobson [1] then Porat [2] showed that the three-dimensional Fourier transform of a sequence in translation is zero except for a plane plane passing through the origin. The slope of this plane is proportional to the apparent velocity components v_x and v_y. Wilson [10] then Oddershede [11] developed several estimators to estimate this slope. Other frequency transforms have been studied in the literature, for example the 3D Gabor transform by Reed [12] and the 3D Cosine transform by Božinović [13]. In this article, we propose an original approach based on spatiotemporal filtering to estimate the apparent velocity vector for each pixel of the sequence of B-mode images. The spatiotemporal volume of data (2D+t) is filtered to estimate the slope. The velocity can then be deduced from it.

The next section presents the method and then provides details on the data used for validation. The results obtained will be presented in section 3 then discussed in section 4. Finally, we will conclude and provide perspectives to our work.

2. MATERIALS AND METHOD

2.1 Method

A 2D+t sequence of images (Fig.1) is considered as a volume called spatiotemporal space (xyt) represented in Fig.2.

Consider in a first time an object in translation along x with a velocity v_x. Then we can write $s(x,t) = s_0(x - v_x t)$ with $s_0(x) = s(x,0)$ the first temporal value. The 2D Fourier transform of $s(x,t)$ is given by Eq. (1):

$$S(F_x,F_t) \quad = S_0(F_x)\delta(F_x v_x + F_t) \tag{1}$$

with $S_0(F_x)$ the Fourier transform of $s_0(x)$. Thereby the Fourier spectrum of an object in translation along one direction is concentrated on a line passing through the origin and satisfying Eq. (2):

$$F_t = -F_x v_x \tag{2}$$

The slope of this line is proportional to the velocity v_x. Resulting from the processing of experimental data, Fig.3a-c shows Fourier transform of several (x,t) planes with different velocities. It corroborates the fact that energy is concentrated on a line whose orientation depends on the velocity. Note that the lines are slightly thick because of the texture of the ultrasonic images; they can be considered as ellipses.

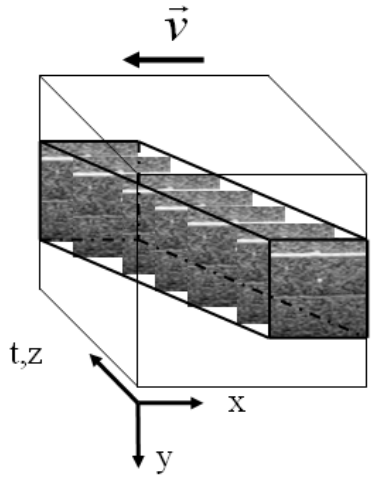

Figure 1: Sequence of images

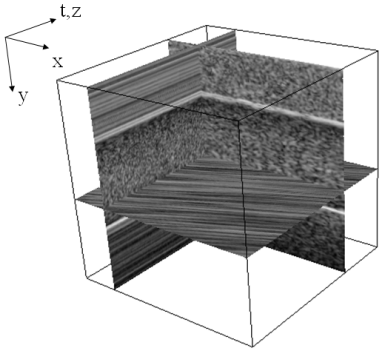

Figure 2: Spatiotemporal space (xyt)

Fig.3a is the Fourier transform of a plane whose velocity is zero whereas Fig.3c is the Fourier transform of a plane with a maximum velocity.

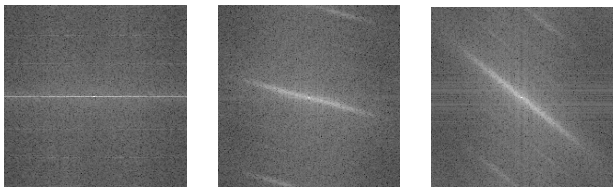

a) b) c)

Figure 3: Fourier transform of several planes with different velocities; abscissa is Fx and ordinate is Ft

The velocity of the object depends on the orientation θ of the line in the (Fx,Ft) plane according to Eq. (3):

$$v = \frac{F_t}{F_s} tan\,\theta \qquad (3)$$

with F_t the temporal frequency (frame rate) and F_s the spatial frequency (spatial sampling).

Thus, the problem of velocity estimation becomes a problem of slope estimation with an angle θ from the Fx-axis. In order to estimate the angle θ, we investigated an approach with banks of oriented [14] Gabor filters. The basic frequency expression of Gabor filter is given by Eq. (4):

$$G(f_x, f_t) = exp\left(-2\pi^2((f_x - f_{x_0})^2\sigma_x^2 + (f_t - f_{t_0})^2\sigma_t^2)\right) \quad (4)$$

The spatial Gabor filter [15] is the product between a Gaussian function with standard deviations of σ_x, σ_y and a sinusoidal wave whose central frequency is f_0. The frequency expression of Gabor filter is then a Gaussian function of width inversely proportional convolved with two Dirac located in $\pm f_0 = \sqrt{f_{x_0}^2 + f_{t_0}^2}$. To design a bank of oriented filters, Eq. (4) must be modified. The orientation of the Gaussian part with angle θ led us to Eq. (5), which is the basic form of an oriented Gabor filter:

$$G(f_x, f_t) = exp\left\{-2\pi^2\left(\sigma_x^2(f_x' - f_0)^2 + \sigma_t^2 f_t'^2)\right)\right\} \qquad (5)$$

with

$$\begin{cases} f_x' &= f_x.cos\,\theta + f_t.sin\,\theta \\ f_t' &= -f_x.sin\,\theta + f_t.cos\,\theta \end{cases}$$

The different adjustable parameters are the angle θ, the standard deviations σ_x, σ_y and the central frequency f_0.

For ultrasound images, the content of the Fourier spectrum of a spatiotemporal plane (x,t) (Fig.3) is mainly located around zero. The frequency selectivity, controlled by the sinusoidal part of Gabor filter, is not necessary. So a null frequency filtering can be chosen setting $f_0 = 0$. Finally, a bank of 2D filters (Fig.4) is designed by setting σ_x and σ_y adapted to ultrasound images and choosing a set of θ uniformly spread on $[0, 2\pi]$:

$$\begin{cases} \theta &= \left(0, \frac{\pi}{4}, \frac{\pi}{2}, \frac{3\pi}{4}\right) \\ \sigma_x &= 10 \\ \sigma_y &= 1 \end{cases}$$

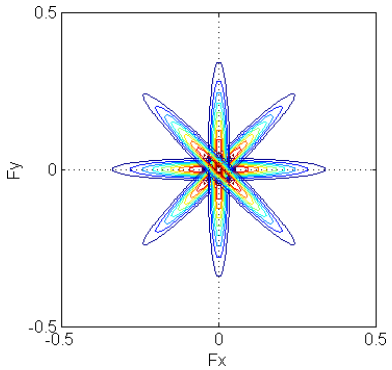

Figure 4: Example of a bank of four oriented filters

We can note that the filters present a central symmetry and therefore the range for θ can be reduced between $[0, \pi]$. To estimate the orientation of the line of the Fourier spectrum, it is successively multiplied with each of the bank's filters. An energy criterion makes it possible to decide which angle θ is the best candidate. From this value of θ, the velocity is deduced from Eq. (3). A multiplication in the fourier domain is equivalent to a convolution in the spatial domain.

The filtering is realized in the spatial domain to avoid the computation of a lot of Fourier transforms.

Consider in a second time an object in translation in the plane (x,y). The velocity consists of two components v_x and v_y so $s(x,y,t) = s_0(x - v_x t, y - v_y t)$. Porat [2] showed that the 3D Fourier transform of $s(x,y,t)$ is given by eq. (6):

$$S(F_x,F_y,F_t) = S_0(F_x,F_y)\delta(F_x v_x + F_y v_y + F_t) \quad (6)$$

with $S_0(F_x,F_y)$ the Fourier transform of $s_0(x,y)$. The spectrum is so concentrated on a plane satisfying Eq. (7):

$$F_t = -F_x v_x - F_y v_y \quad (7)$$

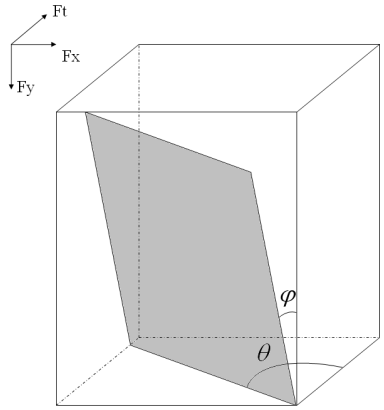

Figure 5: Schematic representation of the plane described in Eq. (7)

Fig.5 represents the tilted plane defined by Eq. (7). Fig.6 shows several slices (Fx,Ft), at different values of Fy, extracted from the 3D Fourier transform of a sequence (experimental data) with moving object. By considering these slices stacked up, the plane in Eq. (7) can be reconstructed as in Fig.5.

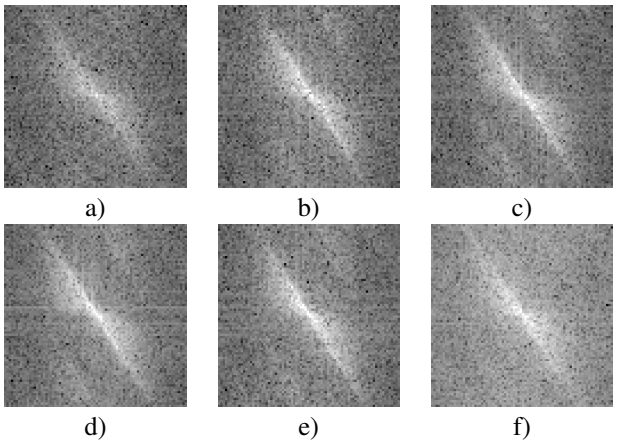

Figure 6: Slices (Fx,Ft) extracted from the 3D Fourier transform of a real sequence; abscissa is Fx and ordinate is Ft

The orientation of this tilted plane is proportional to the velocity components v_x and v_y. It becomes necessary to estimate a second angle φ to compute the two components. From θ and φ, the velocity components are deduced according to Eq. (8):

$$\begin{cases} v_x = \dfrac{F_t}{F_x} tan\,\theta.cos\,\varphi \\ v_y = \dfrac{F_t}{F_y} tan\,\theta.sin\,\varphi \end{cases} \quad (8)$$

To estimate the two angles θ and φ in the volume, we use the extension in 3D of our previous filter (Eq. (5)) according to Eq. (9):

$$G(f_x,f_y,f_t) = exp\left\{-2\pi^2\left(\sigma_x^2 f_x''^2 + \sigma_y^2 f_y''^2 + \sigma_t^2 f_t''^2\right)\right\} \quad (9)$$

with

$$\begin{cases} f_x'' = f_x.cos\,\theta cos\,\varphi + f_y.cos\,\theta sin\,\varphi - f_t.sin\theta \\ f_y'' = -f_x.sin\,\varphi + f_y.cos\,\varphi \\ f_t'' = f_x.sin\,\theta cos\,\varphi + f_y.sin\,\theta sin\,\varphi + f_t.cos\theta \end{cases}$$

Fig.7 presents two examples of 3D oriented frequency filters whose characteristics are:

$$\begin{cases} (\theta,\varphi) = (0,0), \left(\frac{\pi}{3},\frac{\pi}{6}\right) \\ \sigma_x = 10 \\ \sigma_y = 1 \\ \sigma_z = 1 \end{cases}$$

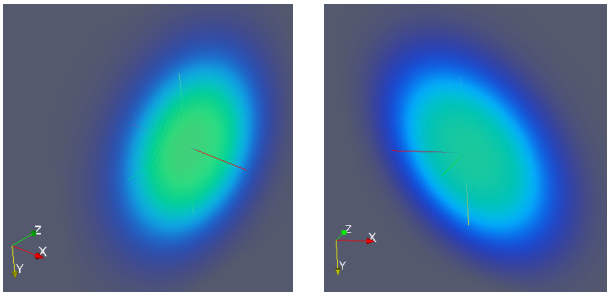

Figure 7: Representation of 3D filters whose characteristics are $\sigma_x = 10$, $\sigma_y = 1$, $\sigma_y = 1$, a) $\theta = 0$ and $\varphi = 0$ b) $\theta = \pi/3$ and $\varphi = \pi/6$

The 3D filters of Fig.7 have the shape of a disk that is well adapted to the planes that we want to estimate. The 3D filters are oriented according to two angles. Fig.7a represents the frequency response of a filter with $\theta = 0$ and $\varphi = 0$. In this case, the plane defined in Eq .(7) is located on the right side of the cube represented in Fig.5. It is merged with the plane (Ft,Fy). Thus, the filter in Fig.7a is particularly adapted to it. Similarly, the filter in Fig.7b is adapted to the grey plane represented in Fig.5.

The method is explained from a macroscopic point of view. However, the Fourier transform can be calculated for each point of the sequence with a small neighbourhood. Each Fourier transform will present a specific slope related to the local velocity. The filtering is then realized locally to estimate the velocity for each pixel of the sequence of B-mode images.

2.2 Materials

2.2.1 Phantom and blood mimicking fluid

A phantom in gelatin was used to simulate the biological tissues. Silica was added to the constitution of the phantom to replace scatterers. A blood vessel, 1 mm in diameter, was placed inside the phantom. As described in [16], blood-mimicking fluid was used as the circulation medium in the vessel. The fluid consists of $5\mu m$ diameter nylon scattering particles (Orgasol, ELF, Atochem, Paris, France) suspended in a fluid base of water, glycerol, dextran and surfactant. The fluid was filtered and degassed before being injected into the flow circuit setup. [16] showed that the fluid's characteristics (density, viscosity, ultrasound propagation velocity and attenuation) were close to the characteristics of human blood. The blood-mimicking fluid was injected into the vessel using a motor-controlled pump (Pump 11, Harvard Apparatus). The mean velocity was less than 1 mm/s.

2.2.2 Ultrasound imaging system

An ultrasonic system (Vevo 660, VisualSonics, Totonto) operating at 40MHz is used to acquire B-mode sequences of 300 images at 30 frames per second. Axial and lateral resolutions are respectively equal to $40\mu m$ and $80\mu m$. Fig.2 in section 2.1 shows a 3D view of the spatiotemporal volume with three orthogonal slices.

3. RESULTS

The results obtained on several sequences are presented; the first one is a sequence with lateral velocity equal to 0.4 mm/s. The second one is a sequence with an oriented vessel with mean velocity equal to 0.55 mm/s. We note that the fluid used in this sequence was not the blood-mimicking fluid but a true blood rabbit. The theoretical parabolic profile in the vessel provided a continuous set of velocities from 0 to $v_{max} = 1.5 * v_{mean}$ at the centre according to the laminar flow situation.
The estimation results on the sequence with $v_{mean} = 0.4mm/s$ are presented in Fig.8 and those on the sequence with $v_{mean} = 0.55mm/s$ in Fig.9. Fig.8a. shows a dense field of velocities and Fig.8b an associated velocity profile (means and standard deviations calculated along the time dimension). Twenty images were used along the time dimension to calculate the profile. An estimate was realized for each pixel of each frame in the region of interest. Thus, it was possible to construct a dynamic color flow mapping (CFM). Fig.9 shows a velocity vector mapping on a B-mode image of the sequence.

Two measures were defined to estimate the quality of the estimates. The first one is the mean error defined in Eq. (10):

$$\overline{E} = \frac{1}{N}\sum_{i=1}^{N}\left(\frac{|\widehat{v_i} - v_i|}{v_{mean}}\right) \tag{10}$$

with $\widehat{v_i}$ the velocity estimated at depth i, v_i the theoretical value according to the parabolic profile and v_{mean} the mean velocity of the flow. The second measure is the mean standard deviation defined in Eq. (11):

$$\overline{std} = \frac{1}{N}\sum_{i=1}^{N}\left(\frac{\widehat{std_i}}{v_{mean}}\right) \tag{11}$$

where $\widehat{std_i}$ is the standard deviation calculated at depth i.

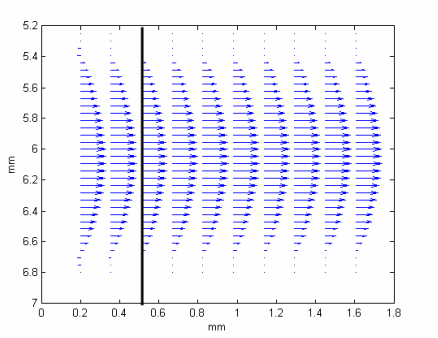

a)

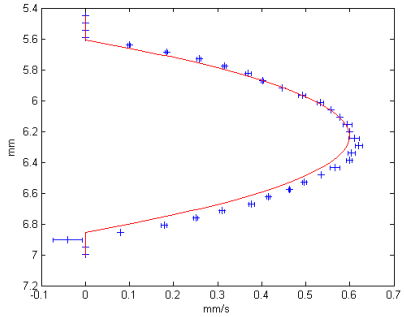

b)

Figure 8: a) Dense field of velocity vectors b) Velocity profile constructed from the black line

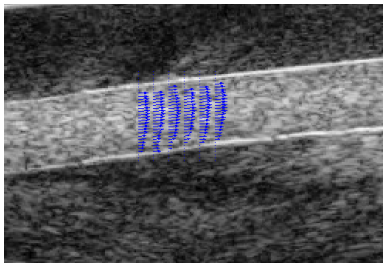

Figure 9: Velocity vector mapping

4. DISCUSSION

Estimates were made on flow sequences with mean value equal to approximately 0.4 mm/s and 0.55 mm/s. Means and standard deviations were calculated from 20 temporal images.
The velocity estimates are close to the theoretically predicted values. For the sequence with $v_{mean} = 0.4\,mm/s$, the mean error between the estimated and theoretical profiles is less than 5.4% and the mean standard deviation is less than 2.1%. For the sequence with $v_{mean} = 0.55\,mm/s$, the mean error and the mean standard deviation are equal to approximately 10%.
We ran into a number of limitations while implementing the method. The first involves the filter kernel size. It cannot be too large because of the temporal decorrelation, which is considered equal to few frames. However, the decorrelation hinges upon the impulse response of the system but also the velocity of the fluid. Therefore, the decorrelation is different depending on the spatial location in the vessel. The filter

kernel size cannot be too narrow because of the discretization. The filter size used is less than 21*21*21 voxels, which provides approximately an angular resolution equal to one degree. The desired angular resolution specifies a minimum size of the kernel. A compromise must be found to account for the decorrelation generated by the velocity and the accuracy desired.

Another limit to the method involves the tangent function relating v and θ (Eq.3), which has a highly non-linear behavior for angles close to 90°. Consequently, the difference in velocity estimations with 85° and 84° (roughly 17%) is greater than that between 32° and 31° (roughly 4%). Thus, it appears essential to work with textures whose orientations are less than 70° in order to have an acceptable level of precision on the estimation. If accurate velocity estimation is critical, it is possible to increase the frame rate or decrease the spatial sampling frequency so that it is placed in the proper zone of the tangent function.

The algorithm is divided into two steps: filtering of the data and computation of the criterion to decide which is the better couple of angles (θ, φ). The computational complexity depends on the number of filters used and the hoped resolution for the results. The time needed to compute estimates into a ROI of 100*100 pixels with our method is approximately 251 seconds. For comparison, the time needed with a standard block matching method is approximately 273 seconds. These methods are both time-consuming. The characteristics of the personal computer used are a Core 2 Duo processor (2.66GHz) and 2Gb of RAM. The calculative cost can be reduced by limiting the results resolution and improving the implementation.

5. CONCLUSION

We proposed in this paper a new blood velocity estimation method based on a Fourier approach. The estimation of the slope of the Fourier spectrum allows us to estimate its velocity by using a bank of oriented filters. First results are encouraging since Doppler techniques cannot be applied to the situation described here. Indeed, low velocities cannot be estimated using Doppler techniques. Furthermore, the method presented provides the two velocity components for each pixel of the sequence. Finally, the method provides good estimates for sequences whose angle between the vessel and the probe axis is near 90°, whereas Doppler techniques are limited to angles less than 60°.

Numerous perspectives are considered and particularly about the implementation. The algorithm is not currently real-time. The use of a bank of filters allows to envisage the parallelization of the algorithm and then the reduction of the calculative time.

Acknowledgements

We wish to thank S. Foster and A. Needles from Sunnybrook Health Sciences Center, Toronto, Canada, where the experiments were conducted. We also thank the french ministry of higher education and research for financial support.

REFERENCES

[1] L. Jacobson and H. Wechsler, "Derivation of optical flow using a spatiotemporal-frequency approach," *Comp. Vis., Graph., and Imag. Proc.* , vol. 38, pp. 29–65, 1987.

[2] B. Porat and B. Friedlander, "A frequency domain algorithm for multiframe detection and estimation of dim targets," *IEEE Trans. Pat. Anal. Mach. Intel.*, vol. 12, pp. 398–401, 1990.

[3] C. Kasai, K. Namekawa, A. Koyano and R. Omoto, "Real-time two-dimensional blood flow imaging using an autocorrelation technique," in *IEEE Trans. Son. Ultras.*, vol. 32, pp. 458–463, 1985.

[4] J.A. Jensen and P. Munk, "A new method for estimation of velocity vectors," in *IEEE Trans. Ultras., Ferro., Freq. Contr.*, vol. 45, pp. 837–851, 1998.

[5] L.N. Bohs, B.J. Geiman, M.E. Anderson, S.C. Gebhart and G.E. Trahey, "Speckle tracking for multidimensional flow estimation," in *Ultrason.*, vol. 38, pp. 369–375, 2000.

[6] A. Basarab, H. Liebgott, F. Morestin, A. Lyshchik, T. Higashi, R. Asato and P. Delachartre, "A method for vector displacement estimation with ultrasound imaging and its application for thyroid nodular disease," in *Med. Im. Ana.*, vol.12, pp.259–274, 2008.

[7] E.I. Céspedes, C.L. de Korte, A.F.W. Van der Steen, "Echo decorrelation from displacement gradients in elasticity and velocity estimation," in *IEEE Trans. Ultras., Ferro., Freq. Contr.*, vol. 46, pp. 791–801, 1999.

[8] W. Aoudi, H. Liebgott, A. Needles, V. Yang, F.S. Foster and D. Vray, "Estimation methods for flow imaging with high frequency ultrasound," in *Ultrason.*, vol. 44, pp. 135–140, 2006.

[9] C. Stiller and J. Konrad, "Estimating motion in image sequences: A tutorial on modeling and computation of 2D motion," in *IEEE Sig. Proc. Mag.*, vol. 16, pp. 70–91, 1999.

[10] L.S. Wilson and R.W. Gill, "Measurement of two-dimensional blood velocity vectors by the ultrasonic speckle projection technique," in *Ultrason. Imaging*, vol. 15, pp. 286–303, 1993.

[11] N. Oddershede, L. Løvstakken, H. Torp and J.A. Jensen, "Multi-dimensional spectrum analysis for 2-D vector velocity estimation," in *IEEE Proc. Int. Ultras. Symp 2007*, New-York, USA, October 28-31. 2007, pp. 2433–2437.

[12] T. R. Reed, "The analysis of motion in natural scenes using a spatiotemporal/spatiotemporal-frequency representation," in *IEEE Proc. ICIP 1997*, Santa Barbara, USA, October 26-29. 1997, pp. 93–96.

[13] N. Božinović and J. Konrad, "Motion analysis in 3D DCT domain and its application to video coding," in *IEEE Sig. Proc.: Imag. Com.*, vol.20, pp.510–528, 2005.

[14] W.T. Freeman and E.H. Adelson, "The design and use of steerable filters," in *IEEE Trans. Pat. Anal. Mach. Intel.*, vol. 13, pp. 891–906, 1991.

[15] J. Kamarainen, V. Kyrki and H. Kälviäinen, "Invariance properties of Gabor filter-based features - Overview and applications," in *IEEE Trans. Ima. Proc.*, vol. 15, pp. 1088–1099, 2006.

[16] K.V. Ramnarine, D.K. Nassiri, P.R. Hoskins and J. Lubbers, "Validation of a new blood-mimicking fluid for use in Doppler flow test objects," in *Ultrasound in Med. Bio.*, vol. 24, pp. 451–459, 1998.